JOURNAL OF GEOPHYSICAL RESEARCH, VOL. 111, C10003, doi:10.1029/2005JC003402, 2006

Quasi-stationary jets transporting surface warm waters across the transition zone between the subtropical and the subarctic gyres in the North Pacific

Osamu Isoguchi,[1] Hiroshi Kawamura,[1] and Eitarou Oka[2,3]

Received 18 November 2005; revised 1 May 2006; accepted 15 June 2006; published 3 October 2006.

[1] Surface flow jets and associated sea surface temperature (SST) distribution are investigated in the northwestern North Pacific, using satellite-derived surface currents and SST data that can resolve fine spatial scale structure. The combined use of these data reveals warm tongue phenomena driven by surface geostrophic jets, which extend northeastward in the Kuroshio-Oyashio transition area. They roughly coincide with the Subarctic Front (SAF) defined as the 4°C isotherm at 100 m depth. The phenomena appear throughout the year with seasonal cycles, which do not correspond with that of the subarctic North Pacific. Their positions are affected by bottom topography so that their quasi-stationary and consistent features are suggested. Thus it is implied that these jets play an important role in transporting warm waters toward the subarctic region. The time series of SST and current fields describe the jets' year-to-year variability involving some changes in strength and connections with the Kuroshio Extension (KE), and demonstrate the effects of advection by the jets on SST fields. When KE extends northward at its crests for 1999–2002, one of the jets along SAF simultaneously strengthens, resulting in high SST region directly over and along the south side of the jet. Hydrographic data show warm, saline water intrusions along the jets. Their mean fields also reveal that these jets are vertically well-developed, forming a boundary between the subtropical and subarctic gyres in the North Pacific.

Citation: Isoguchi, O., H. Kawamura, and E. Oka (2006), Quasi-stationary jets transporting surface warm waters across the transition zone between the subtropical and the subarctic gyres in the North Pacific, *J. Geophys. Res.*, *111*, C10003, doi:10.1029/2005JC003402.

1. Introduction

[2] The Kuroshio and the Oyashio are the western boundary currents of the subtropical and subarctic gyres in the North Pacific. The Kuroshio-Oyashio transition area east of Japan is an ocean area where they converge. Complex oceanic features such as complicated frontal structures appear and various water masses are formed [e.g., *Yasuda*, 2003]. In addition, this area is known as one of the most important fishing grounds. Thus the Kuroshio-Oyashio transition area is thought to be an important region for the understanding of climate and ecosystem variations. This region is sometimes referred as the Mixed Water Region (MWR). MWR is defined as the area between the northern edge of the Kuroshio Extension (KE) and the Subarctic Front (SAF), defined as the 4°C isotherm at 100 m depth [*Favorite et al.*, 1976].

[3] Several major fronts such as SAF, the Subarctic Boundary (SAB), and the Kuroshio Bifurcation Front (KBF) have been defined in this region, on the basis of hydrographic observations [e.g., *Favorite et al.*, 1976; *Mizuno and White*, 1983]. *Zhang and Hanawa* [1993] and *Yuan and Talley* [1996] have given comprehensive discussions about frontal structures and their variability in the North Pacific by using climatological data and synoptic surveys. They gave better understanding about frontal structure. However, the detailed description of their horizontal distribution and connection was not researched enough due to limitations on the temporal/spatial resolution of the hydrographic data. In addition, although oceanic jet is one of the principal factors in the formation of these fronts, distinct relation between the fronts and the flow fields was not adequately described. Recently, the accumulation of historical observations, new observation technology, and high-resolution numerical simulations have made it possible for us to investigate the detailed structure related to flow fields. *Qu et al.* [2001] have constructed new hydrographic climatologies in a 0.5° × 0.5° grid to investigate time-average structure of the Kuroshio/Oyashio system east of Japan, and have revealed the detailed structure associated with the narrow western boundary currents. *Iwao et al.* [2003] have derived intermediate flow fields in the

[1]Center for Atmospheric and Oceanic Studies, Graduate School of Science, Tohoku University, Aoba, Sendai, Miyagi, Japan.
[2]Institute of Observational Research for Global Change, Japan Agency for Marine-Earth Science and Technology, Yokosuka, Kanagawa, Japan.
[3]Ocean Research Institute, University of Tokyo, Tokyo, Japan.

0148-0227/06/2005JC003402$09.00

Table 1. Summary of the SST Products Used in This Study

Products	Spatial Coverage	Spatial Resolution	Temporal Coverage	Temporal Resolution	Other	Reference
NGSST	13–63°N, 116–166°E	0.05°	Feb 2003–Dec 2004	Daily	Cloud-free	*Guan and Kawamura* [2004]
OI SST	Global	0.1°	Jan 1993–Jun 2003	Daily	Cloud-free	*Kawai et al.* [2006]
4 km AVHRR Pathfinder	Global	4 km	1993–2004	5 day		(http://www.nodc.noaa.gov/sog/pathfinder4km/userguide.html)
9 km AVHRR Pathfinder Climatology (CSST)	Global	9 km		5 day	Climatology	*Armstrong and Vazquez-Cuervo* [2001]

Kuroshio-Oyashio transition area from the trajectories of subsurface floats. They have investigated the formation, distribution, and synoptic scale circulation structure of the North Pacific Intermediate Water (NPIW), which is characterized as a salinity minimum distributed in the subtropical North Pacific [e.g., *Talley*, 1993].

[4] The KE's bifurcation has been studied based on observations and numerical simulations, because its northern branch connects to the SAF and gives a significant impact on heat transports into the subarctic region. *Mizuno and White* [1983] have revealed from the synoptic thermal fields at a 300 m depth that KE often bifurcated at 150–165°E. *Levine and White* [1983] have demonstrated that mean strong thermal fronts divided into two separate bands over the Shatsky Rise and that the northern band kept heading northeastward along the Shatsky Rise, eventually connecting to SAF. *Sainz-Trapaga et al.* [2001] have estimated by combining altimeter and hydrographic data with a two-layer reduced gravity model that KE's bifurcations occurred for the range between 147°E and 160°E. This bifurcation over the Shatsky Rise has been simulated with a numerical model [e.g., *Hurlburt and Metzger*, 1998]. They pointed out that the high-resolution model and realistic bottom topography are essential to reproducing the bifurcation.

[5] The advance of satellite observations allows us to investigate spatially/temporally high-frequency phenomena on an ocean surface and has given improved knowledge about the Kuroshio-Oyashio transition area. Using satellite infrared (IR) images and intensive hydrographic observations, the detachment process of eddies from the Kuroshio Extension (KE) and an eddy-eddy interaction have been described in detail as a short-term variation [*Kawamura et al.*, 1986; *Yasuda et al.*, 1992]. In addition, geostrophic warm streamers and warm tongues, separating from KE, which are sometimes called the secondary Kuroshio Front [*Kawai*, 1972], have been investigated [e.g., *Kawai and Saitoh*, 1986]. These phenomena are directly related to not only the supply of warm water from KE into MWR but also the northward migration of pelagic fish and fishing grounds [e.g., *Kawai and Saitoh*, 1986; *Sugimoto and Tameishi*, 1992]. However, the connection between the secondary Kuroshio Front, SAF, and the Subarctic Current has not been elucidated clearly [*Kawai*, 1972].

[6] The accumulation of satellite SST observations over 20 years makes it possible to analyze phenomena with a fine spatial scale, such as fronts and streamers, at climatological points of view. Moreover, altimeter-derived sea surface height (SSH) measurements over 10 years can extract surface current fields on a scale of 100 km. As for hydrographic structure, almost all climatologies in the North Pacific have been constructed by applying some smoothing procedures due to sparse observations, especially in the open ocean. Thus they don't necessarily have enough information to describe the fine spatial structure related to fronts and jets. Hydrographic measurements have recently increased dramatically, even in such a gap region, with the aid of the global deployment of profiling floats, known as Argo [e.g., *Argo Science Team*, 2001]. These data lead to the construction of the hydrographic mean fields, which preserve structure as finely as possible.

[7] In this study, by using satellite-based SST and surface current data, and historical hydrographic observations, surface jet streams and associated SST phenomena are investigated in the Kuroshio-Oyashio transition area. They reveal the existence of warm tongues driven by quasi-stationary jets, which suggests that these jet streams can be a possible consistent mechanism to transport the subtropical water into the northern region. In section 2 the data used are described. The analyzed results including the extraction of the warm tongues driven by quasi-stationary jets, their temporal variability, and hydrographic structure related to the jets are presented in section 3. Section 4 gives summary and discussions.

2. Data

2.1. Satellite-Based Observations

[8] Several satellite-based SST products, which are summarized in Table 1, are used in this study. The New Generation Sea Surface Temperature (NGSST) data (http://www.ocean.caos.tohoku.ac.jp/~merge/sstbinary/actvalbm.cgi?eng=1) are quality-controlled, cloud-free, and high-spatial resolution (0.05°-grided) products. They are SST generated daily by objectively merging the satellite SST observations from infrared radiometers and a microwave radiometer [*Guan and Kawamura*, 2004]. The satellite-based global daily 0.1°-grid SST data [*Kawai et al.*, 2006], which are produced by applying the optimum interpolation (OI) method (hereinafter OI SST), are also used. They have a relatively longer time period from January 1993 to June 2003.

[9] The 4 km Advanced Very High Resolution Radiometer (AVHRR) Pathfinder Version 5.0 SST Project (Pathfinder V5) is a new reanalysis of the AVHRR data stream developed by the University of Miami's Rosenstiel School of Marine and Atmospheric Science (RSMAS) and the NOAA National Oceanographic Data Center (NODC), distributed in partnership with the NASA Physical Oceanography Distributed Active Archive Center (PO.DAAC) (http://www.nodc.noaa.gov/sog/pathfinder4km/userguide.html). In this 4 km Pathfinder project, the AVHRR data has

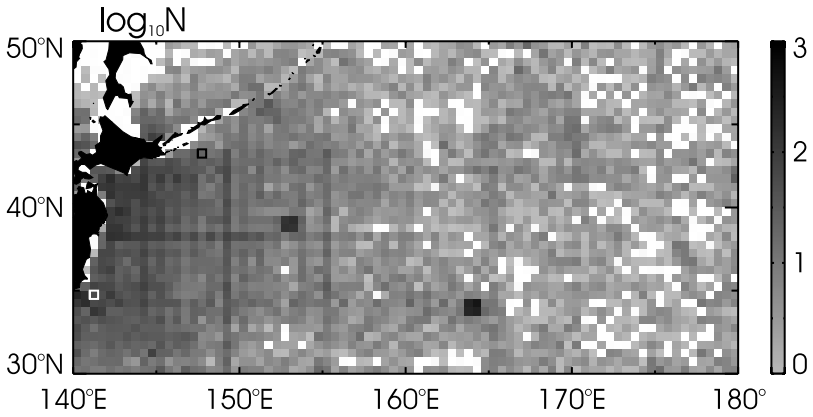

Figure 1. The distribution of the number of hydrographic observations at each 0.5° × 0.5° grid. The values are expressed in a common logarithm. The white grids mean no data. Pure Kuroshio and Oyashio water profiles, which are depicted in Figure 13, are derived at the grids surrounded with white and black lines, respectively.

been reprocessed at the 4 km Global Area Coverage (GAC) level, the highest resolution possible. We use the 5-day average product (hereinafter, 5-day SST) for 12 years, 1993–2004. The data for 2002 is, however, still an interim version.

[10] We also use the AVHRR Pathfinder Global 9 km Pentad SST Climatology (hereinafter, CSST) [*Armstrong and Vazquez-Cuervo*, 2001] as a global high resolution climatology. The CSST pentad climatology consists of 73 fields representing the mean annual cycle of SST with 5-day resolution. It was derived from the daily Pathfinder SST time series from 1985–1999. Gaussian interpolation was applied to interpolate the satellite data into 5-day pentads onto a 9 km grid to create a global high resolution climatology.

[11] Altimeter data is used in this study to estimate surface flow fields. They are maps of sea level anomaly (SLA) obtained from "Segment Sol multimissions d'ALTimétrie, d'Orbitographie et de localisation précise/Data Unification and Altimeter Combination System (SSALTO/DUACS) Delayed Time Sea Level Anomalies (DT-MSLA)". These were constructed for the period from October 1992 to January 2005 with a 7-day interval, by merging the SLA observations of the ocean TOPography Experiment (TOPEX)/Poseidon and European Remote Sensing satellite (ERS)-1/2 or those of Jason-1 and ENVISAT. No ERS data are used between January 1994 and March 1995. The grid interval is a MERCATOR 1/3°, which means that resolutions in kilometers in latitude and longitude are identical and vary with the cosine of latitude (from 37 km at the equator to 18.5 km at 60°N/S). The detail of data processing has been described by *Ducet et al.* [2000].

[12] In this study, we estimate upper ocean steric signals due to the seasonal cycle of heating and cooling within the oceanic mixed layer and remove them from SSHA. Following *Stammer* [1997], the thermosteric signals (η'_{heat}) are estimated using net surface heat flux data as

$$\eta'_{heat}(t) \approx \eta'_{heat}(t_0) + \frac{1}{\rho_o c_p}\int_{t_0}^{t} \alpha_T (Q_{net} - \langle Q_{net}\rangle)dt', \qquad (1)$$

where ρ_o, c_p are the reference density and the specific heat of seawater, and are defined as constant values. $\alpha_T (= \rho^{-1}\,\partial\rho/\partial T)$ is the thermal expansion coefficient which spans 1×10^{-4} to 3×10^{-4} °C^{-1} for ocean. Q_{net} is the net surface heat flux, which is also collected from the NCEP/NCAR Reanalysis. $\langle Q_{net}\rangle$ means a time averaging value. α_T is derived from monthly temperature and salinity fields from *Levitus and Boyer* [1994] and *Levitus et al.* [1994]. Mixed layer depth is determined as the depth having the potential density greater by 0.125 sigma-theta than that at the surface, and then α_T is calculated from the mean temperature and salinity averaged over the mixed layer depth. Thus monthly thermosteric height signals are calculated on a 1° × 1° grid over the North Pacific and the monthly SSHA relative to the steric signals are calculated.

2.2. Hydrographic Observations

[13] For hydrographic mean fields, the North Pacific HydroBase (hereinafter NPHB) [*Macdonald et al.*, 2001] updated by *Suga et al.* [2004] is used. The updated NPHB has been supplemented by some profiles of *World Ocean Atlas 1994* [*NODC*, 1994], the CTD data from several World Ocean Circulation Experiment (WOCE) sections and pre-WOCE sections, and the CTD data collected by National Oceanic and Atmospheric Administration/Pacific Marine Environmental Laboratory (NOAA/PMEL) [*Johnson and McPhaden*, 1999]. We use 27215 profiles for the range, 140°–180°E, 30°–50°N. In addition to the NPHB data, 7736 temperature and salinity profiles measured from January 2001 to July 2005 by the Argo profiling floats, which cover the same range as the NPHB data, are used. These data were downloaded from Argo's two Global Data Assembly Centers in Brest, France (ftp://ftp.ifremer.fr/ifremer/argo/) and Monterey, California (ftp://usgodae1.fnmoc.navy.mil/pub/outgoing/argo/). Using analysis tools included in *HydroBase 2* (http://www.whoi.edu/science/PO/hydrobase), about 35000 potential temperature and salinity profiles from NPHB and Argo are isopycnally averaged onto 0.5° × 0.5° grids. Figure 1 shows the numbers of the averaged profiles within each 0.5° × 0.5° grid. By the addition of the Argo float data, substantial blank grids in the NPHB data are filled, especially in the region east of 160°E. Though the blank grids

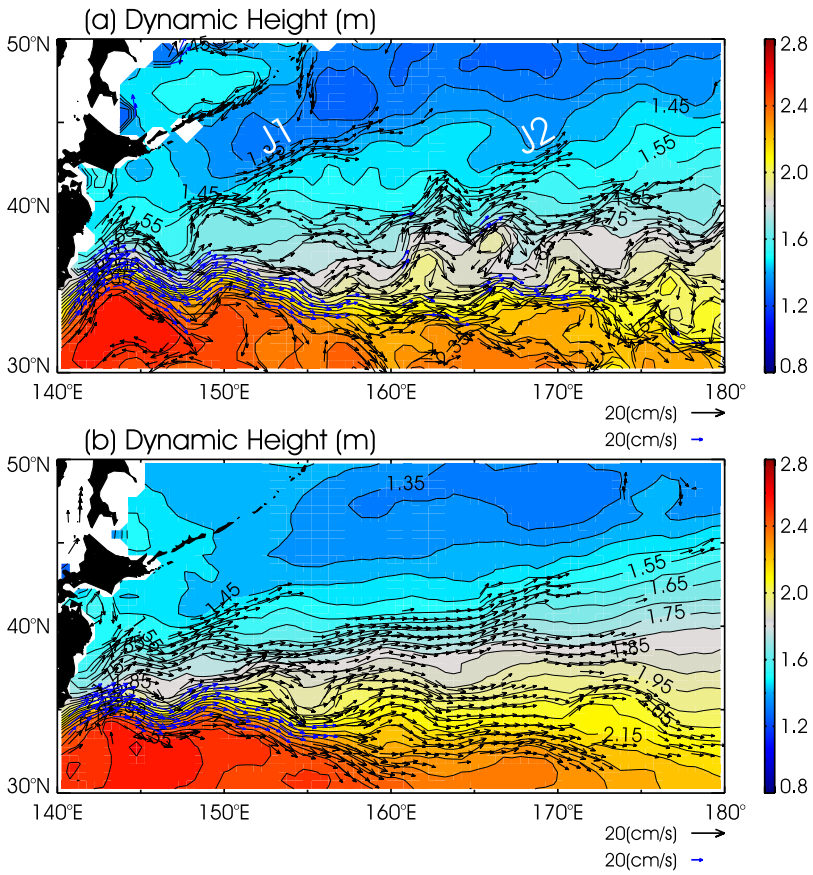

Figure 2. Climatological mean sea surface heights (SSH) relative to 1500 dbar and surface currents larger than 7 cm/s, which are (a) calculated in this study and (b) derived from *Kuragano and Shibata* [1997]. Units are meter and a contour interval is 0.05 m. The surface currents larger than 20 cm/s are rescaled and shown with blue arrows. Their references are shown below each figure. J1 and J2 in Figure 2a denote the jets investigated in this study.

shown in white in Figure 1 still remain, some of them are isopycnally interpolated by an iterative Laplacian/spline algorithm with a searching radius of 2°. On the other hand, some blank grids, which do not meet the criterion of the radius of 2°, are left as a gap. In this study, the mean property fields are constructed without a heavy smoothing procedure to preserve spatial structure as finely as possible, although some gaps and noisier structure are left.

[14] In addition, climatological SSH relative to 1500 dbar is calculated on the 0.5° × 0.5° grid from these potential temperature and salinity profiles. Before the dynamic computation, these profiles are smoothed along isopycnals with a 5-point Laplacian filter included in *HydroBase 2*. Figure 2a shows the computed SSH superimposed with surface geostrophic currents larger than 7 cm/s. Large surface velocities (>20 cm/s) are rescaled and shown in gray. The strongest jet is KE, where the quasi-stationary meander with the first and second crests at about 144°E and 150°E [e.g., *Kawai*, 1972; *Mizuno and White*, 1983], is clearly depicted. Along with it, the mean SSH averaged for 1993–1998 [*Kuragano and Shibata*, 1997], which is obtained from the data set CD-ROM of the Subarctic Gyre Experiment (SAGE) project [*Japan Meteorological Agency*, 2001], is shown in Figure 2b. *Kuragano and Shibata*'s [1997] mean SSH has been calculated by combining altimeter and hydrographic observations. Dynamic height relative 1500 dbar is first calculated from each observation profile. Then, the mean SSH for the altimeter observing period is estimated at each point by subtracting altimeter-derived SSHA, which is acquired at near time and location. This method has an advantage that the mean SSH at the hydrographic observation points can be constructed by at least one observation during the altimeter observing period. An error in the constructed SSH has been estimated to be less than 2 cm in most areas [*Kuragano and Shibata*, 1997]. The SSH constructed in this study shows noisier structure than *Kuragano and Shibata*'s [1997] mean SSH and probably retains the effect of instantaneous hydrographic structure, especially in areas without sufficient observations. Nevertheless, two northeastward surface jets (lettered as J1 and J2 in Figure 2a) heading into the subarctic region, which are the main subject in this paper, exist at almost the same locations in both the mean SSH fields constructed from different source data. The mean SSH we computed (Figure 2a) is applied in the following analyses because its surface current fields related to KE's bifurcations and their relationship with bottom topography, which is shown later, are closer to the thermal front structure [*Levine and White*, 1983] and the SSH and associated current fields recently constructed by a combination of altimeter and subsurface

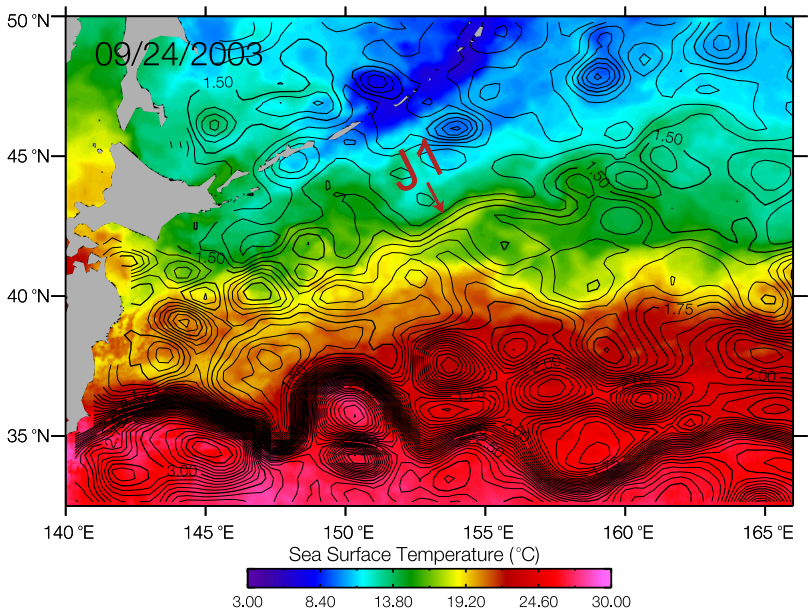

Figure 3. A snap shot of sea surface temperature (SST) on September 24, 2003. Sea surface height (SSH) contours (contour interval of 0.05 m with 0.25 m thickened) are superimposed. The location of a warm tongue is indicated by "J1".

drifter data [*Niiler et al.*, 2003]. For reference's sake, we performed the same analyses with *Kuragano and Shibata*'s [1997] mean SSH and got essentially the same conclusion in terms of the above two jets. Based on the mean SSH, we construct synthetic SSH every 7 days by adding SSHA, and then calculate surface geostrophic velocities.

[15] The winter mixed layer climatology of the North Pacific [*Suga et al.*, 2004] is also obtained from the same SAGE data set CD-ROM [*Japan Meteorological Agency*, 2001]. It is also calculated from the NPHB dataset by averaging original observations within the smallest possible area around a grid point to preserve realistic water properties of a mixed layer, especially in frontal regions [*Suga et al.*, 2004].

3. Results

3.1. Warm Tongues Driven by Quasi-Stationary Surface Jets

[16] Warm streamers or tongues that spread northeastward in the Kuroshio-Oyashio transition area are frequently confirmed from the animated images of NGSST and OI SST (not shown). These high SST bands are almost parallel with the iso-lines of the synthetic SSH. Figure 3 shows a snap shot of the NGSST on September 24, 2003, on which the synthetic SSH contours are superimposed. A warm water band, which protrudes northeastward from around 150°E, 40°N, can be seen (indicated by "J1"). The warm water band runs, to some extent, parallel to the SSH contours of 1.45–1.55 m with relatively steep horizontal gradients, which implies the relationship of the warm band with surface geostrophic flows. *Kawai and Saitoh* [1986] have described a warm tongue and a geostrophic warm streamer, based on satellite images and hydrographic observations. They pointed out that these are unified as a warm water band transported northward by a geostrophic jet stream without any countercurrent components inside the warm water band. Their typical dimensions are a depth of 50–170 m and width of 60–100 km for the warm tongue, and a depth of 25–50 m and width of 35–70 km for the geostrophic warm streamer. In this study, the warm band and a similar one are, for the sake of convenience, called a warm tongue because of a lack of hydrographic information. Good correspondence in each snap image implies enough ability of the satellite-derived SST and SSH data to investigate oceanic phenomena with high-spatial resolution (∼several tens of kilometers) in the Kuroshio-Oyashio transition area.

[17] In order to detect the mean picture of the warm tongues and their relation with surface currents, the climatologies of SST (CSST) and SSH are analyzed. A spatially high-pass filter is applied for the respective 5-day CSST data to extract fine spatial structure (∼several tens of kilometers). First, CSSTs are smoothed with a low-pass filter with an e-folding scale of 0.75° (hereinafter, LCSST) and then high-pass filtered CSST anomaly (hereinafter, HCSST) is derived by subtracting LCSST from the original CSST. The 73 5-day HCSSTs are then averaged (Figure 4a). The mean picture of HCSST still shows a northeast-southwest warm band from 148°E, 39°N to 155°E, 43°N, which is likely to correspond to the warm tongue in Figure 3. In addition, another warm band is confirmed east of the former one, lying on the tilt from 165°E, 40°N to 170°E, 42°N.

[18] The surface mean currents (>7 cm/s) shown in Figure 2a are superimposed on the HCSST map. For references, the Subarctic Front (SAF), which is defined as the 4°C isotherm at 100 m depth [*Favorite et al.*, 1976], is estimated from the constructed mean temperature fields and superimposed with blue lines (Figure 4a). The abovementioned relatively distinct jet streams with northeastward flow (J1 and J2 indicated in Figure 2a) are roughly parallel with SAF north of 40°N. In addition, the position of J1 and

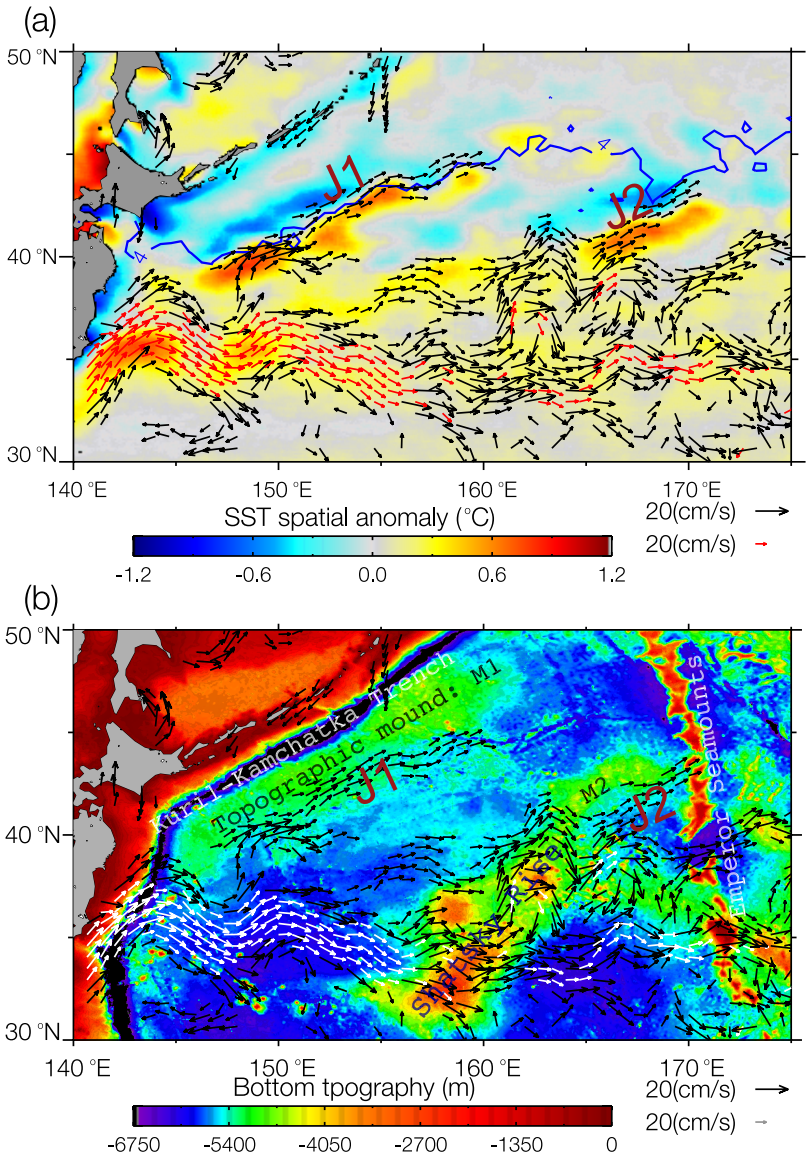

Figure 4. (a) The climatology of spatially high-pass filtered SST anomalies. Mean surface currents larger than 7 cm/s are superimposed with arrows, where large velocity vectors (> 20 cm/s) are red and rescaled. Velocity vector scales of 20 cm/s are shown on the right side of the scale bar. Blue lines are 4°C isotherms at 100 m depth, which is a definition of the Subarctic Front. (b) Bottom topography along with the strong surface currents (>7 cm/s). The location of J1 and J2 is indicated.

J2 approximately corresponds to the warm bands discussed above. J1 is generally recognized as the Subarctic Current. At the same time, Figure 4a indicates that J1 is related to warm water at least in the surface layers.

[19] The existence of the 2 jets discussed above has been recently pointed out by the direct measurements [e.g., *Niiler et al.*, 2003; *Iwao et al.*, 2003]. *Niiler et al.* [2003] have provided near-surface current fields in the KE region by using 657 drifters deployed during 1989–2001. They described mean flow fields related to not only KE but also two prominent jets in the Kuroshio-Oyashio transition area: one along the eastern slope of the topographic mound (M1; see Figure 4b) east of the Kuril-Kamchatka (KK) Trench, and the other along 38°–40°N that turns to the north at 165°E, 40°N. They seem to correspond to J1 and J2 in this study. Their current field presents that mean flow speed along both the jets reaches up to 20–30 cm/s. *Iwao et al.* [2003] have presented intermediate current fields on the 26.7 σ_θ surface in the northwestern North Pacific by using 21 subsurface floats deployed for 1998–2002. They pointed out three types of strong eastward flows: 1) KE at 32°–35°N, 2) the Subarctic Current at 42°–45°N, and 3) the flow along the subarctic boundary at 39°–40°N. Judging from their figure, the second and a part of the third flows correspond to J1 and J2. Their figure shows that mean velocities on the 26.7 σ_θ surface, which is equivalent to almost 200–300 m depths at 40°–45°N, are almost 15 cm/s and 5–7 cm/s for J1 and J2, respectively.

[20] The positions of J2 as well as J1 are likely to be related to bottom topography. Figure 4b shows the mean surface current field (>7 cm/s), which is superimposed on the bottom topography derived from a global digital eleva-

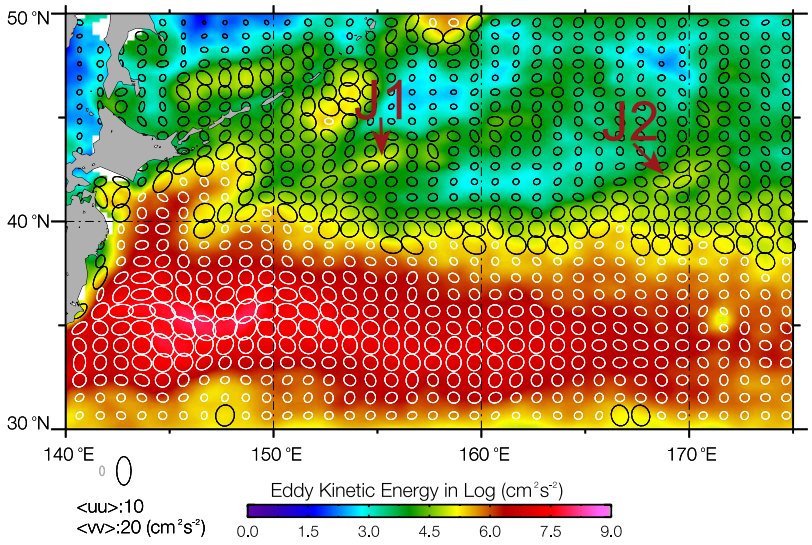

Figure 5. The distribution of mean eddy kinetic energy (EKE), on which Reynolds' stress ellipses are superimposed. The Reynolds stress ellipses are drawn in two scales and colors. The reference of each scale is shown on the left side of the scale bar. The location of quasi-stationary jets is indicated.

tion database originally developed by the U. S. Defense Mapping Agency (ETOPO5). The figure, on the whole, shows the effect of bottom topography on the route of the strong jets. KE bifurcates over the Shatsky Rise around 160°E and one part of them heads northeastward along the Shatsky Rise. This is consistent with the observational results by *Mizuno and White* [1983] and *Levine and White* [1983], who have defined the bifurcation routes with synoptic thermal maps. The numerical simulation configured with realistic topography has also reproduced the bifurcation over the Shatsky Rise and the mechanism of the bifurcation has been investigated by *Hurlburt and Metzger* [1998]. The other strong jets passing through the Emperor Seamounts tend to selectively converge on the relatively deep gaps such as 43°N, 39°N, and 34°N.

[21] J1 is, as pointed out by *Niiler et al.* [2003], parallel with the eastern slope of M1. J2 seems to have a connection with a part of the KE bifurcations and is mainly parallel with the eastern slope of the topographic mound of the northern part of the Shatsky Rise (M2; see Figure 4b). *Niiler et al.* [2003] hypothesized the strong current could have a strong barotropic component. In a series of numerical experiments, *Hurlburt et al.* [1996] have successfully simulated these jets and pointed out that bottom currents produced by baroclinic instabilities interact with bottom topography and in turn steer the surface currents. While the available data is not sufficient to test these hypotheses, the point here is that the quasi-stationary feature of these jets is attributed to bottom topography.

[22] Each snap shot of SST and SSH shows that warm water seems to be transported by geostrophic warm streamers or warm tongues into MWR via several anti-cyclonic eddies, which distribute in the area, especially west of 155°E [e.g., *Kawamura et al.*, 1986; *Yasuda et al.*, 1992]. One might suspect that the averaging process of these eddies artificially produces the quasi-stationary jets. Figure 5 shows the mean eddy kinetic energy (EKE) map with the Reynolds stress ellipses, which are calculated from the altimeter-derived surface current anomalies. EKE is expressed in a natural logarithm and the Reynolds stress ellipses are drawn with two scales. High EKE areas along KE and Oyashio are prominent. They are probably attributed to the KE jet and mesoscale eddies detached from it, and the Oyashio and eddies propagating on the trench [*Isoguchi and Kawamura*, 2003], respectively. Meanwhile, the relatively high EKE streaks appear along J1 and J2. The principal axes of the Reynolds stress ellipses along these streaks are approximately parallel to the directions of the jets. Interestingly, gentle regions can be seen on both sides of these active streaks. In particular, a lower EKE patch surrounded with the higher EKE regions, which is located on the southeast side of J1 (157–164°E, 41–43°N), is prominent. These results support the idea that the high variability along the two jets north of 40°N is mainly attributed not to propagating disturbances like eddies, but to the quasi-stationary feature of surface currents.

3.2. Annual Cycles of the Jets

[23] Figure 6 shows seasonal (3 months) mean HCSSTs with seasonal mean flows larger than 7 cm/s (left figures) and seasonal mean SSHs (right figures). J1 and the associated warm tongues are persistent through the year, while they, at the same time, show some seasonal features. The SSH maps show that some SSH contours concerning J1 are connected with the Western Subarctic Gyre (WSAG), forming return flows as the Subarctic Current, while a part of them is also connected with the northern extent of the crests of the KE meander. In particular, this feature is clearer in summer and fall, as described later. Some effects of the subtropical gyre on J1 are thus inferred from the SSH maps. Moreover, it has been reported as a short-term phenomenon that the secondary Kuroshio Front transports warm waters northward as geostrophic warm tongues and streamers via anticyclonic eddies, which exist at any time in MWR [e.g., *Kawai*, 1972; *Kawai and Saitoh*, 1986]. It is hypothesized that these eddies systematically transport the effect of KE to the quasi-stationary jet, J1.

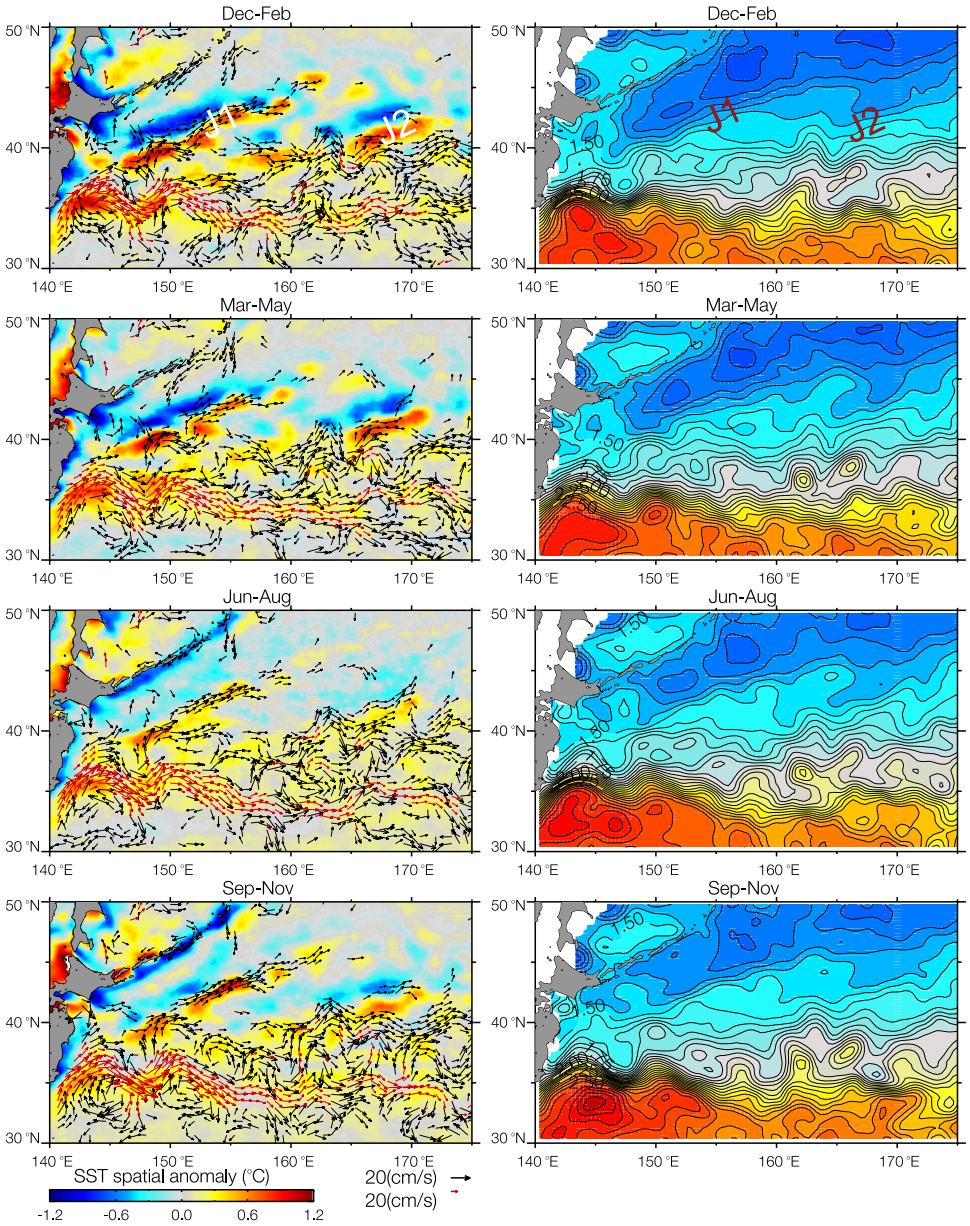

Figure 6. The seasonal (3 months) mean maps of (left) spatially high-pass filtered SST anomalies, on which seasonal mean surface currents (>7 cm/s) are superimposed, and (right) the synthetic SSHs. Large velocity vectors (>20 cm/s) in the left figures are red and rescaled. Velocity vector scales of 20 cm/s are shown on the right side of the scale bars. The contour interval of SSH is 0.05 m, and the location of quasi-stationary jets is indicated in the upper maps.

[24] The SSHs in WSAG are relatively lower in winter and spring (upper 2 panels) than in summer and fall, which indicates the wintertime spinning-up of the gyre. This entails the relatively stronger northeastward return flows of the subarctic gyre, widening J1 on the side of the subarctic gyre, which results in covering over the cold SST bands (upper 2 left panels). This is reasonable because the western boundary currents of the subarctic gyre (the East Kamchatka Current and the Oyashio) are strong in winter and spring [e.g., *Uehara et al.*, 1997; *Isoguchi et al.*, 1997]. In summer and fall, on the other hand, the SSHs are relatively higher on the side of the subtropical gyre, which results in developing a steep SSH gradient along J1, in spite of the weaker subarctic gyre. This intensified J1 converges on the warm water bands, implying the northeastward feeding of warm waters as the geostrophic warm tongue. J2, on the other hand, forms relatively clear jets in spring and summer but less in fall and winter. We calculate the temporal variations of J1 and J2 using the hydrographic altimeter-combined surface currents. First, the principal axes of the jets are defined at grids where the mean currents are larger than 7 cm/s (arrows in Figure 4a), inside the ranges of 150–162°E, 40.5–45.5°N and 162–171°E, 40–46°N for J1 and J2, respectively. Then the principal axis components of the altimeter-derived current anomalies are calculated at the selected grids and their means are derived

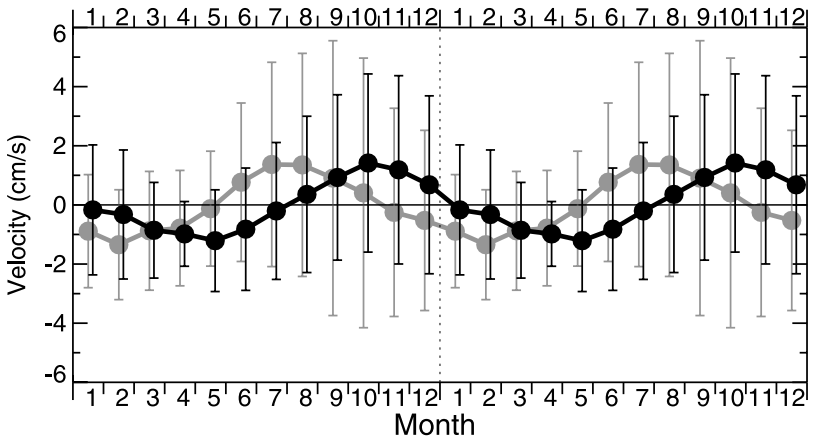

Figure 7. The annual cycles of the J1 (black) and J2 (gray) currents. Error bars denote their standard deviations. Each annual cycle is shown twice side by side.

as the J1 and J2 variations every month for 1993–2004. The annual cycles of the J1 and J2 variations are shown with black and gray lines in Figure 7. The vertical bars show their standard deviations. Although the year-to-year variability, which will be investigated later, seems to be too large, especially about J2, to describe the annual cycles, they show the above mentioned seasonal features, specifically, that J1 (J2) is the most intensified in fall (summer). It is emphasized again that the seasonal cycle of J1 is not consistent with that of WSAG. Thus although J1 is involved more by the return flow of WSAG in winter and spring, the seasonal variation of its strength is not likely to be controlled by WSAG.

[25] One might suspect that the spatial filtering in Figures 4a and 6 artificially generates di-pole banded structure for a strong SST front and the warm bands with cold counterparts in Figures 4a and 6 do not necessarily correspond to warm tongues or streamers. It might be true that averaging process in climatoligical fields makes the banded structure obscure and the di-pole SST bands in Figures 4a and 6 just represent strong SST fronts, especially for J2. If the di-pole represents the SST front, the axis of the jet is expected to be along its node. Nevertheless, the axis of J1 is not along the node but just over the warm band in summer and fall, when J1 is relatively strong. In addition,

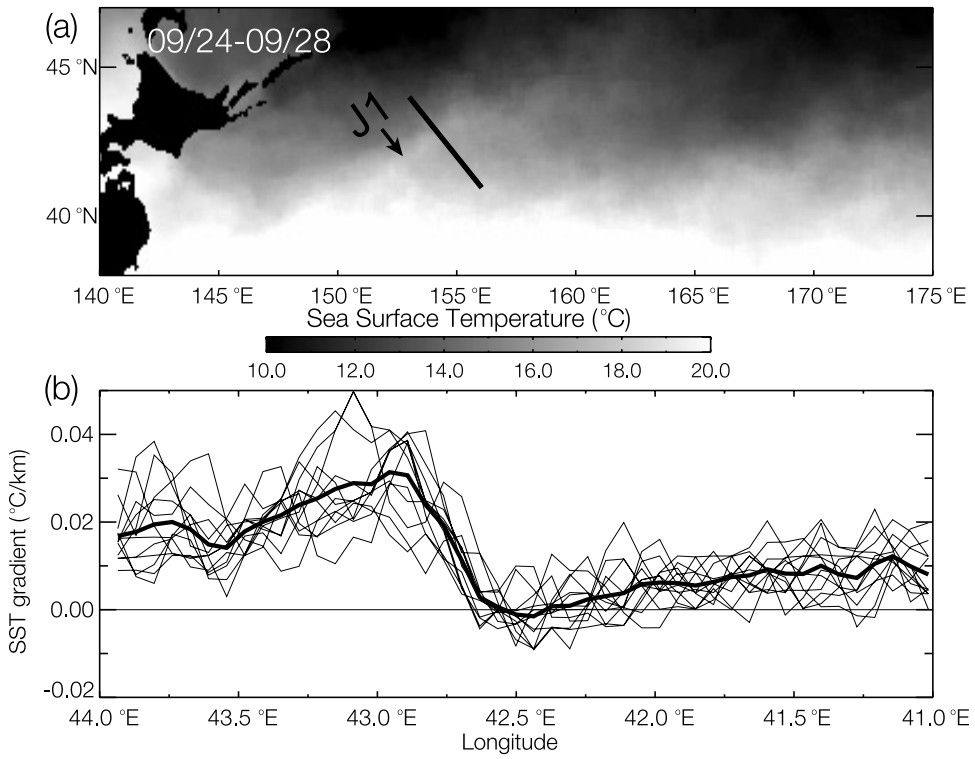

Figure 8. (a) The Pentad SST Climatology [*Armstrong and Vazquez-Cuervo*, 2001] for 24–28 September. The location of J1 is indicated. (b) SST gradient profiles along the black line shown in Figure 7a for September–October (thin lines) and their average (a thick line). They are calculated from the Pentad SST Climatology.

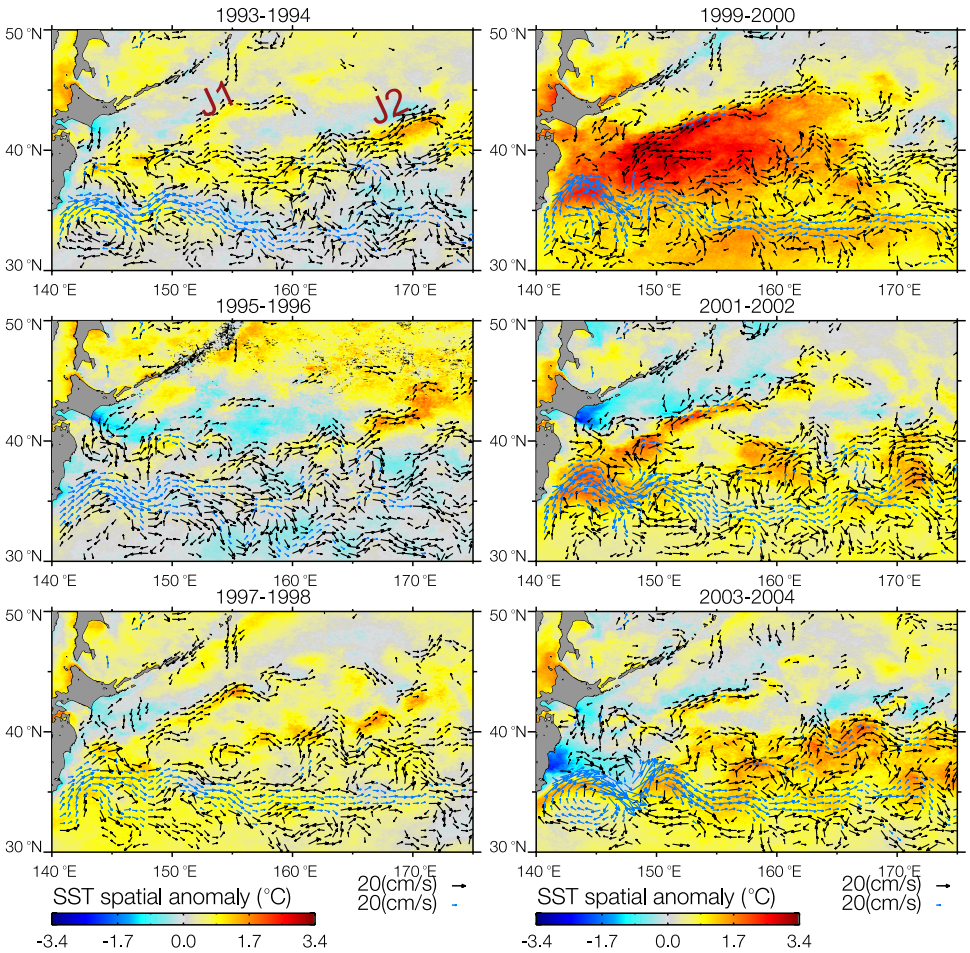

Figure 9. The time evolution of 2 years mean surface currents (>7 cm/s) and SST anomalies, which are derived by subtracting spatially low-pass filtered SST climatology. Large velocity vectors (>20 cm/s) are blue and rescaled. Velocity vector scales of 20 cm/s are shown on the right side of the scale bar. The location of quasi-stationary jets is indicated in the upper left panel.

the original 5-day CSST for 24–28 September (Figure 8a) shows the northeastward intrusions of warm waters at the positions of J1 and J2, although J2 is not as clear as J1. SST gradients along the black line in Figure 8a, which cuts across the warm band concerning J1, are calculated from the 12 CSST fields for September–October and shown (thin lines) along with their average (a thick line) in Figure 8b. Most of the 12 profiles and the average exhibit negative gradients around 42.5°N, which indicates warm banded structure with a center at a zero crossing latitude. Thus the warm banded structure is apparently retained for September–October even in the climatological data constructed from the 15-year data, which indicates the stationary and robust features of J1 and the associated warm tongues.

3.3. Year-to-Year Variability of the Jets and Its Impact on SST Fields

[26] The year-to-year variability of the jets and associated SST fields including the warm tongues are investigated. The 5-day SST anomalies are first calculated by subtracting the low-pass filtered CSST (LCSST) from the 5-day SST time series. In consequence, anomaly components with a small spatial scale, which are related to the warm tongue structure, and those with a large scale, which are mainly caused by the interannual variations of heat fluxes, retain in the 5-day SST anomalies. By using the 5-day data and climatologies instead of monthly mean or longer mean data, phenomena with a small spatial scale are expected to be detected more clearly. These 5-day anomalies are then averaged for 2 successive years and are shown in Figure 9, on which the simultaneous mean surface currents (>7 cm/s) are superimposed. Also shown in Figure 10 is the time evolution of the 2-year mean SSHs. The large-scale SST anomalies over the whole region in Figure 9 are thought to be mainly brought about by the interannual variations of heat fluxes. On the other hand, a notable point is that the year-to-year changes of the warm tongues in strength correspond to those of the jets. J2 is relatively strong during 1993–1996, forming the apparent jet streams and warm tongue structure, while J1 and associated warm tongues are relatively weak. After 1997, J1 strengthens and J2 weakens. At the same time, as seen in Figures 9 and 10, the crests of KE's meander shift northward for 1999–2002, which implies the some connection between the KE jet and J1. As the result of advection by J1, positive SST anomalies appear over and along the south side of J1 in 1999–2002, forming the well-defined SST front along J1. These interannual features are confirmed from the SSH maps (Figure 10):

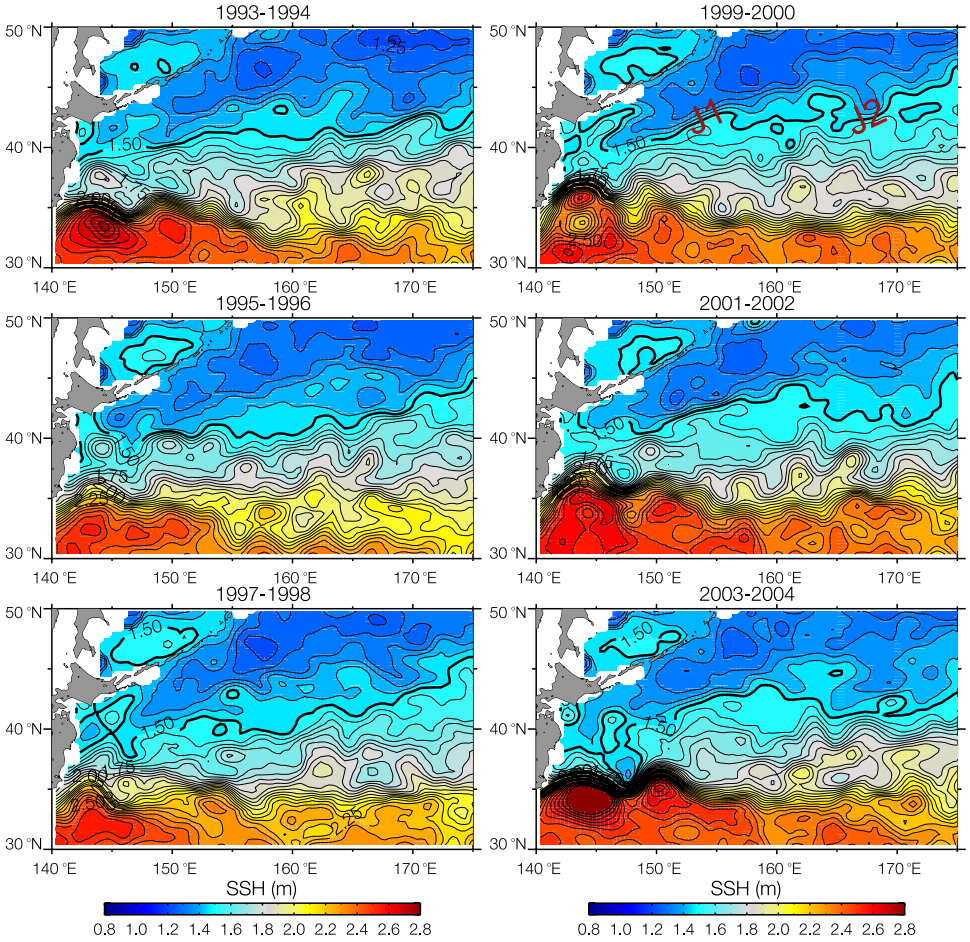

Figure 10. The time evolution of 2 years mean SSH. Units are meters and a contour interval is 0.05 m. The contours of 1.5 m are shown with thick lines. The location of quasi-stationary jets is indicated in the upper right panel.

SSH gradients across J1 (J2) are relatively weak (strong) during 1993–1996, being followed by a gradual strengthening (weakening) after 1997. An interesting point again is that WSAG does not show such clear interannual variations compared with the subtropical gyre. Thus the interannual variation of J1 is mainly attributed not to WSAG but to the SSH change on the southeast side of J1. This is clearly shown by the north-south migration of the 1.5 m contours (thick black lines in Figure 10). The 1.5 m contours move northward after 1997 and are approximately along with J1 after 1999, developing a steep slope across J1. The migration is likely to be consistent with the KE's meridional shift, which will be investigated later.

[27] We examine the above year-to-year variability, focusing on J1 and J2. The interannual anomalies of J1 and J2 relative to their annual cycles (Figure 7) are shown with red and blue lines in Figure 11a. This time evolution describes the low frequency variability shown in Figures 9 and 10. J1 gradually strengthens from 1996 and reaches at its peak for 1999–2001, being followed by weakening after 2002. On the other, J2 basically shows the variation with an opposite phase. The regressed fields of surface current and OI SST anomalies relative to their annual cycles on the interannual variation of J1 (Figure 11a) are calculated (Figure 11b). The OI SST's field is calculated for the temporal period from Jan 1993 to June 2003. The regressed fields on J2 show, on the whole, the opposite patterns of those on J1 (not shown). The regressed current field inevitably leads to a strong and well-defined jet along J1. At the same time, as mentioned above, the northward shift of the KE's meander is expected to occur around its crests east of the Japan coasts. We conveniently define the Kuroshio axis as the 2.0 m contours of SSHs, which roughly correspond to the maximum velocity in the climatological field (Figure 2a), and estimate its time evolution from each monthly map. The latitudinal position of the upstream KE, which is averaged for 142–148°E, is depicted along with the J1 interannual variation (Figure 12). The derived variations of the upstream KE axis are consistent with those detected by B. Qiu and S. Chen (Variability of the Kuroshio Extension jet, recirculation gyre and mesoscale eddies on decadal timescales, submitted to *Journal of Physical Oceanography,* 2006). The correlation between the KE position and J1 is 0.61, which is not necessarily significant to the 95% confidence interval if their low frequency feature is considered. Nevertheless, both the time series approximately show the above mentioned low frequent variation. The J1 and KE's northward shift entail strong positive SST anomalies, spreading northeastward from the crests of the KE's meander to J1 and its south region. This describes that when the crests of the KE's

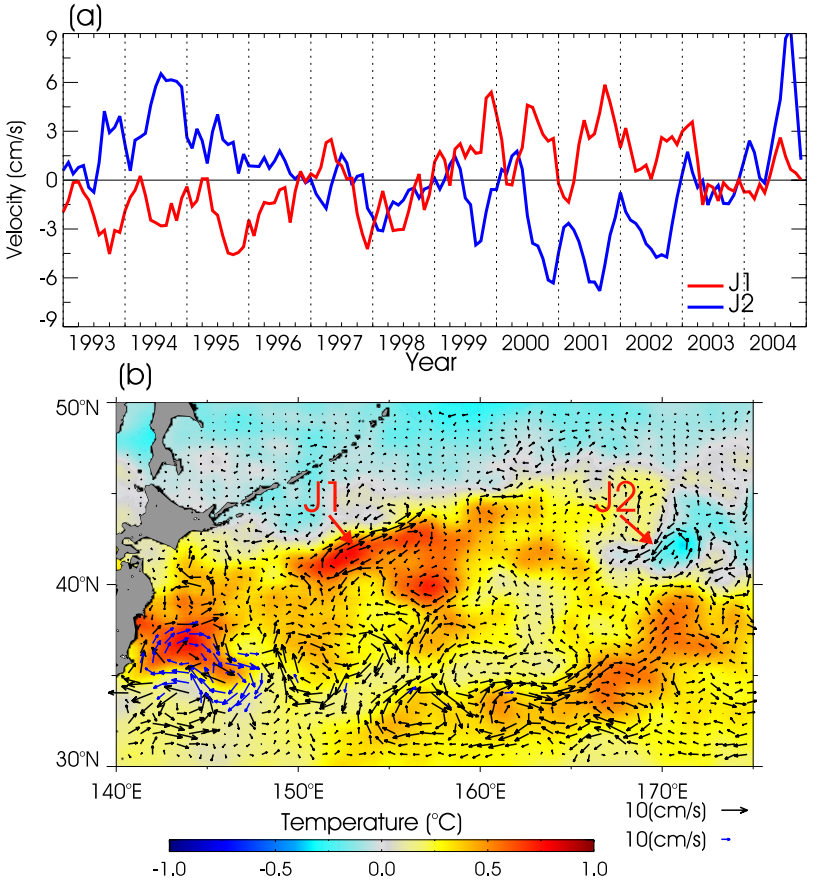

Figure 11. (a) The time series of J1 (red) and J2 (blue) relative to their annual cycles. (b) The regressed maps of SST and surface current anomalies on the J1's interannaul time series. The regressed current larger than 10 cm/s are rescaled and shown with white. The location of J1 and J2 is indicated.

meander extend northward after 1999, J1 and the associated warm tongue structure simultaneously strengthen, indicating that much heat and substance are transported into the northern region. In contrast, J2 tends to weaken (the southwestward arrows) in the same period, entailing the negative SST anomaly. Figure 11 thus suggests some connections between the KE jet, J1, and J2. However, it should be noted that the result just shows the fact that the northward shift of the KE's meander, the strengthening of J1, and the weakening of J2 occur concurrently, at least in this period. Mechanisms controlling the variations of J1 and J2 and their interactions with the KE jet are beyond the scope of this study and should be addressed in the future study, by using high-resolution numerical simulations configured with realistic bottom topography.

3.4. Hydrographic Structure

[28] In this section, the hydrographic mean fields constructed from the historical observations are used to discuss the vertical structures of the jets and their water mass type. *Qu et al.* [2001] have produced similar climatologies from NPHB [*Macdonald et al.*, 2001] in the Kuroshio-Oyashio transition area. In this study, our attention is focused on the phenomena with fine spatial scale that were revealed from the satellite observations. Therefore, we created the mean hydrographic fields, trying to hold spatial structure as finely

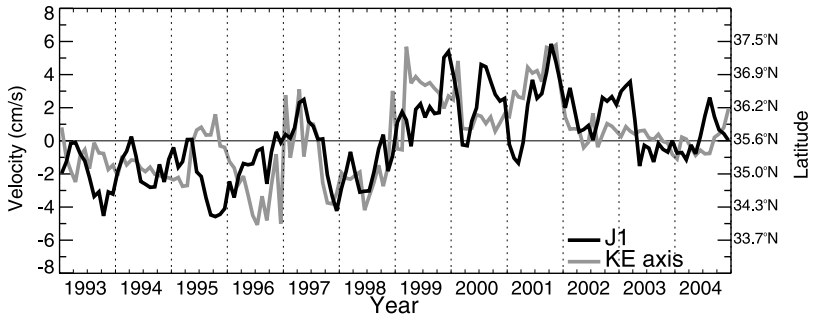

Figure 12. The time series of J1 (black) and the latitudinal position of the upstream KE axis for 142–148°E (gray). The KE axis is determined as the 2.0 m contours of the SSH maps.

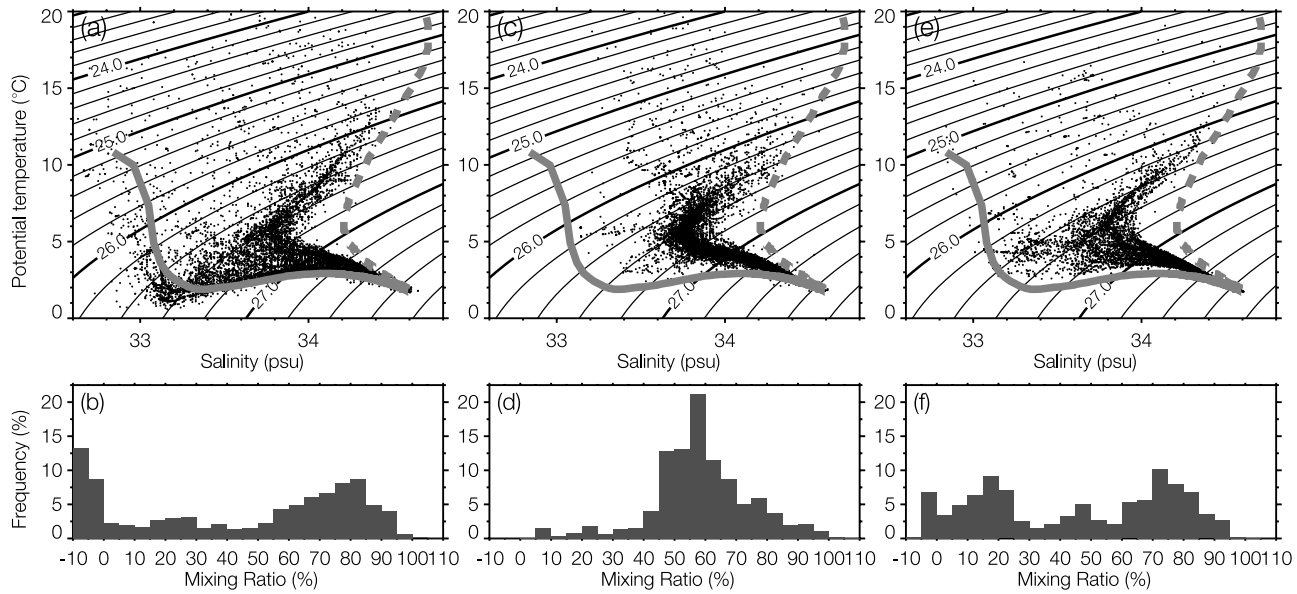

Figure 13. θ - S diagrams in the (a) J1, (c) intermediate, and (e) J2 regions, on which the pure Kuroshio (a dashed gray line) and Oyashio (a bold gray line) water profiles are superimposed. The histograms of the Kuroshio mixing rations for the density range from 26.0 σ_θ to 26.5 σ_θ in the (b) J1, (d) intermediate, and (f) J2 regions. Each region is shown in Figure 14c.

as possible. This is the main difference between this study and the previous analysis.

[29] Following *Zhang and Hanawa* [1993], the Kuroshio mixing ratio is estimated from these hydrographic mean fields to examine the geographical distribution of two typical water masses of the Kuroshio and Oyashio waters. The mixing ratio is defined as,

$$r_\theta(\%) = 100 \times (\theta - \theta_O)/(\theta_K - \theta_O),$$
$$r_S(\%) = 100 \times (S - S_O)/(S_K - S_O), \quad (2)$$

where r_θ and r_S are the mixing ratios for potential temperature, θ, and salinity, S, and θ_O, θ_K, S_O, and S_K are the potential temperature and salinity of the pure Oyashio and Kuroshio waters at an isopycnal surface, σ_θ. Although the two types of the mixing rations are calculated by the definition, their average is used in this study. The pure Kuroshio and Oyashio water properties are selected from the mean θ and S profiles around 141.25°E, 34.75°N, and 147.75°E, 43.25°N, respectively (see Figure 1), where the observation numbers within each grid are relatively large. The respective θ - S profiles are depicted in Figure 13. The Kuroshio mixing ratios are then calculated by the equations (2) every 0.1 σ_θ from 25.5 σ_θ to 27.3 σ_θ.

[30] (a) Potential temperature, (b) salinity, (c) acceleration potential anomaly (geostrophic flow function) [*Montgomery*, 1937] relative to 1500 dbar, and (d) mixing ratio maps on the 26.5 σ_θ surface are depicted in Figure 14. Only the acceleration potential anomaly map is smoothed with a 3 × 3 median filter to reduce noisy structure. The mean currents at the sea surface (>7 cm/s) are superimposed on the acceleration potential map. The contours of 50% are drawn in red on the mixing ratio maps (Figure 14d). Both the potential temperature and salinity maps on the 26.5 σ_θ surface (Figures 14a and 14b) show well-defined northeast-southwest fronts along J1 and J2, due to their compensating nature on an isopycnal surface. In particular, the J1-related northeastward protrusions of warm and saline waters are prominent. The acceleration potential map (Figure 14c) also shows well-defined fronts related to J1 and J2. The 50% contours in the mixing ratio map are generally along with J1 and J2, involving the J1-related protrusion. These results indicate that J1 and J2 form a boundary between the subtropical and subarctic waters, at least on the 26.5 σ_θ surface. In order to investigate the water mass property of each temperature, and salinity profiles around and between J1 and J2, the profiles around J1 and J2 and those between them are plotted on θ - S diagrams (Figures 13a, 13c, and 13e, respectively). Their ranges are shown with red frames and a green square in Figure 14c. The intermediate region shown in the green square corresponds to the lower EKE region on the southeast side of J1 (Figure 5). In addition to that, mixing ratios are calculated for the plots between 26.0–26.5 σ_θ and their histograms with a 5% interval are shown in Figures 13b, 13d, and 13f. For the upper layers lighter than 26.5 σ_θ, which correspond to about 100 m and 150 m around J1 and J2, the plots along J1 and J2 (Figures 13a and 13e) tend to split and converge around both the pure Oyashio and Kuroshio water references (bold and dashed gray lines, respectively). This water mass feature around J1 has been clearly pointed out by simultaneously conducted observations [*Kono*, 1997]. Meanwhile, those in the green square converge on an intermediate position between the pure Oyashio and Kuroshio references (Figure 13c). These tendencies are described well in the histograms of the mixing ratio. The histograms for J1 and J2 (Figures 13b and 13f) have two clusters divided into the Kuroshio and Oyashio water type ranges. The J1's histogram, in particular, reaches a peak at relatively higher Kuroshio mixing ratios of 80–85%. On the other hand, the histogram for the green square (Figure 13d)

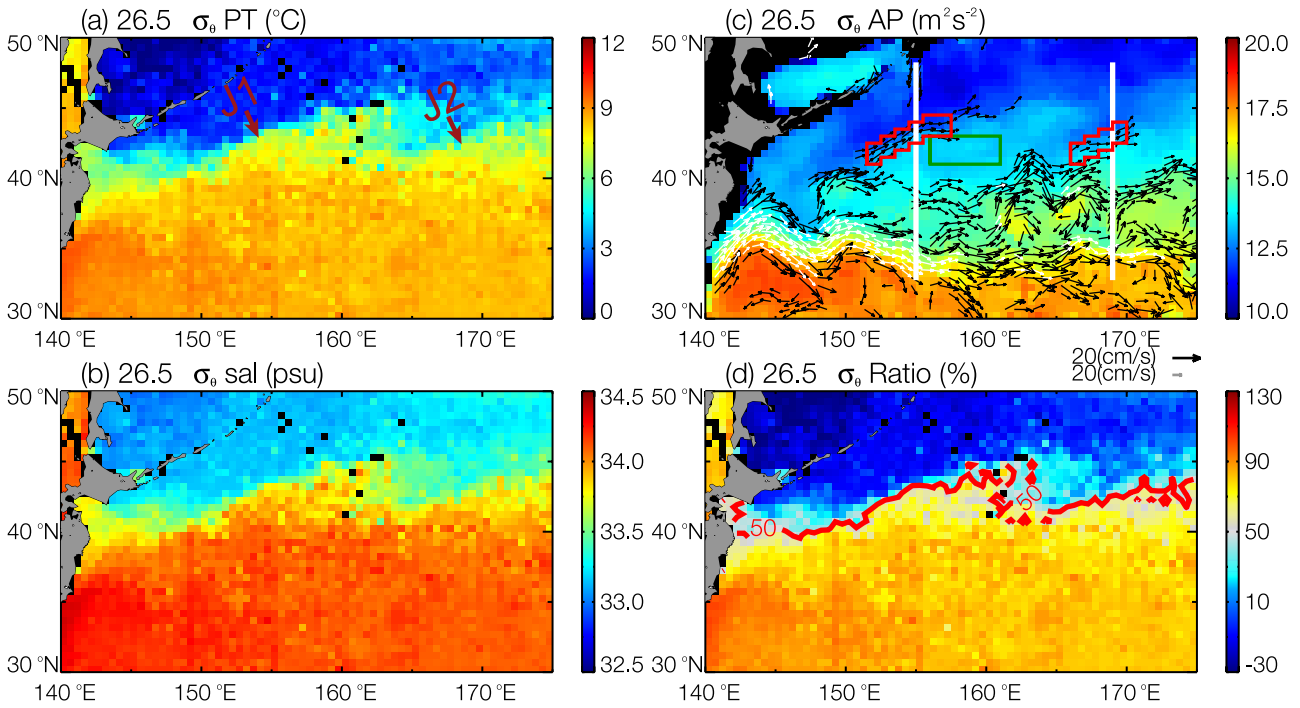

Figure 14. The distributions of (a) potential temperature (°C), (b) salinity (psu), (c) acceleration potential (m^2s^{-2}) relative to 1500 dbar, and (d) the Kuroshio mixing ratio (%) on the 26.5 σ_θ surface. The acceleration potential is displayed after applying a 3 × 3 median filter. The surface mean currents (>7 cm/s) and 155°E and 169°E sections (white lines) are superimposed on the acceleration potential map. Also shown on the acceleration potential map are regions around J1 and J2 (red frames) and between them (a black frame), each observation of which is plotted on the θ - S diagrams in Figure 13. The location of J1 and J2 is indicated in Figure 14a.

just shows a cluster, reaching a peak at 55–60%. It is suggested from the results that, at least for the layers shallower than 26.5 σ_θ, the subtropical warm and saline waters are transported, selectively, by J1 and J2 into the northern region in the northwestern North Pacific.

[31] Figure 15 shows mixing ratio sections along (a) 155°E and (b) 169°E, which cut across the axes of J1, J2, and KE (shown with white lines in Figure 14c). The contours for 10–90% are drawn every 20% with green lines on them. Eastward geostrophic velocities relative to 1500 dbar (> 5 cm/s) and potential density are superimposed with black and white contours. The velocity sections describe the vertical structure of KE, J1, and J2. The eastward flows, corresponding to KE and J1, can be seen at 34°N and 43.5°N in the 155°E section (Figure 15a), while those corresponding to KE and J2 are at 35°N and 43°N in the 169°E section (Figure 15b). J1 and J2 are vertically well developed with the velocity exceeding 5 cm/s down to about 700 m and 600 m. This result supports the idea that the upper layer warm tongues are driven by the consistent geostrophic jet along SAF. The mixing ratio maps show the distinct relationship between J1 and J2 and a water mass boundary. Although the 50% contours shift southward apart from J1 at the lower levels, the 30% contours run almost vertically, forming well-defined fronts at the position of J1 and J2. Thus the contribution of the Oyashio water becomes larger and larger with depth, on the south sides of J1 and J2. These jets are, nevertheless, still a type of boundary between the subtropical and subarctic waters.

[32] As mentioned above, the warm and saline water protrusion into the region north of 40°N can been seen on the 26.5 σ_θ surface (Figures 14a and 14b). According to the acceleration potential map (Figure 14c), intermediate flow along J1 detours around the brink of the protrusion with a northeastern crest around 166°E, 45°N and eventually connects to J2. This detouring route can be seen in the surface flow fields for 1999–2000 and the some SSH maps in Figures 9 and 10. In addition, even on the 26.7 σ_θ surface, most intermediate floats have been reported to depict the detour trajectories with the crest around 166°E, 45°N [see *Iwao et al.*, 2003, Figure 3]. The detour route is roughly consistent with SAF (the 5°C isotherm at 100 m in Figure 4a). These results suggest the existence of the quasi-stationary anticyclonic detour circulation, which forms the northern extent of the subtropical gyre. In fact, the northern extent of J1 and J2, or the associated front of the acceleration potential map, reaches around 45°N, which is consistent with the boundary between the subtropical and subarctic gyres determined from historical wind stress data based on the simple linear Sverdrup theory.

4. Summary and Discussions

[33] In this study, we examined the quasi-stationary jets and the associated warm tongue phenomena in the Kuroshio-Oyashio transition region, by using satellite-derived SST, sea level anomaly (SLA), and surface current data. Then, we discussed the hydrographic structure of the

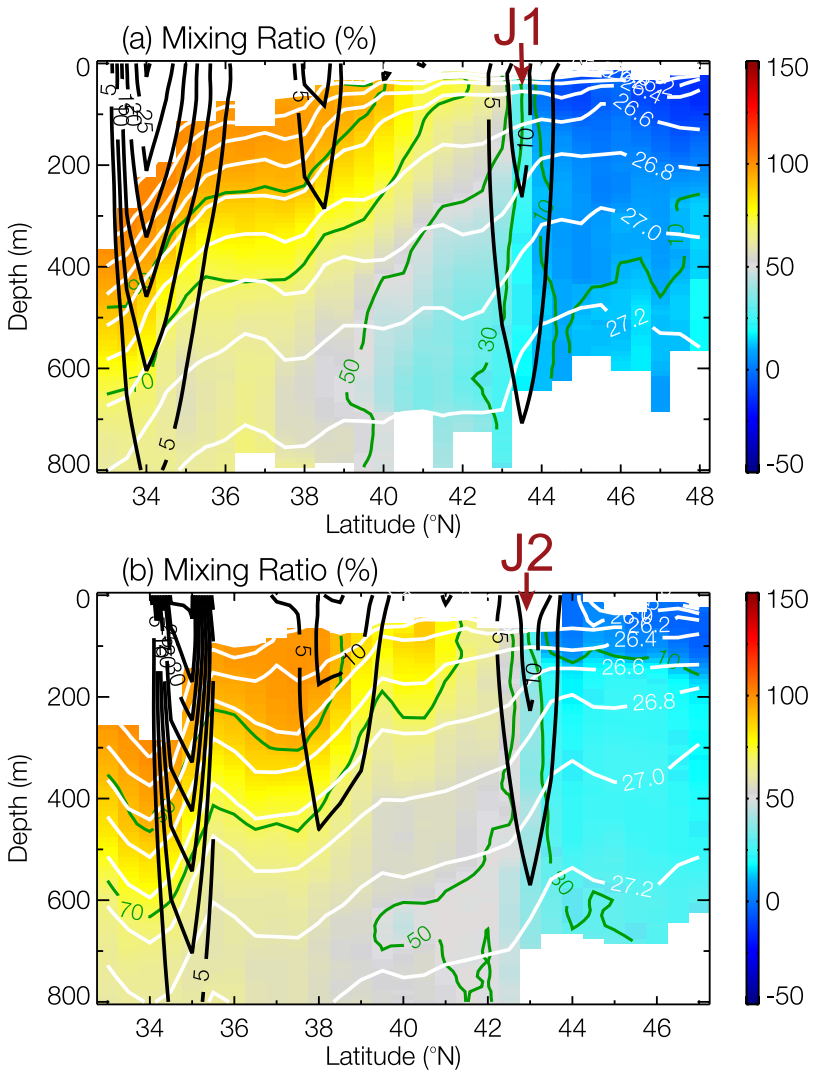

Figure 15. The vertical sections of the Kuroshio mixing ratio (%) along (a) 155°E and (b) 169°E with green contours every 20% form 10% to 90%. Eastward geostrophic current (> 5 cm/s) and potential density (σ_θ) contours are superimposed every 5 cm/s and 0.2 σ_θ. The location of J1 and J2 is indicated.

surface jets, based on the hydrographic mean fields constructed from historical observations. The details are as follows.

[34] The recently constructed cloud-free daily SST data with high spatial resolution [*Guan and Kawamura*, 2004; *Kawai et al.*, 2006] have revealed the warm tongues, frequently spreading northeastward along SAF. These cloud-free SST time series were quite useful for understanding of phenomena with fine spatial structure through the construction of an animated image and a regressed map of SST anomaly on certain time series. The consistency of the warm tongues has been confirmed from the spatially high-pass filtered climatological SST, based on the 1985–1999 Advanced Very High Resolution Radiometer (AVHRR) data. The surface current fields derived from the constructed hydrographic mean field indicated that the warm tongues were driven by the mean geostrophic jets (J1 and J2 shown in Figure 2). J1 and J2 coincided roughly with the surface and intermediate current fields previously constructed by surface drifting buoys [*Niiler et al.*, 2003] and subsurface floats [*Iwao et al.*, 2003]. These geostrophic warm tongues exist throughout the year with a seasonal tendency, being strongest in fall (summer) for J1 (J2). The positions of the jets and warm tongues are governed by bottom topography: they parallel with the eastern slopes of the topographic mounds, as pointed out by *Niiler et al.* [2003]. It is suggested that the quasi-stationary warm tongues driven by the geostrophic jets can be a consistent mechanism transporting surface warm water toward the subarctic region.

[35] The time evolution of the 2-year mean maps of the high-pass filtered SST anomalies, along with the surface currents and sea surface height (SSH), demonstrated that the jets underwent some low frequency changes in strength, and they entailed the corresponding changes of surface thermal structures. The regressed maps of surface currents and SSTs on the J1's interannual time series could describe the following year-to-year variability. When the crests of the KE's meander extended northward in 1999–2001, J1 simultaneously strengthened, resulting in the high SST region

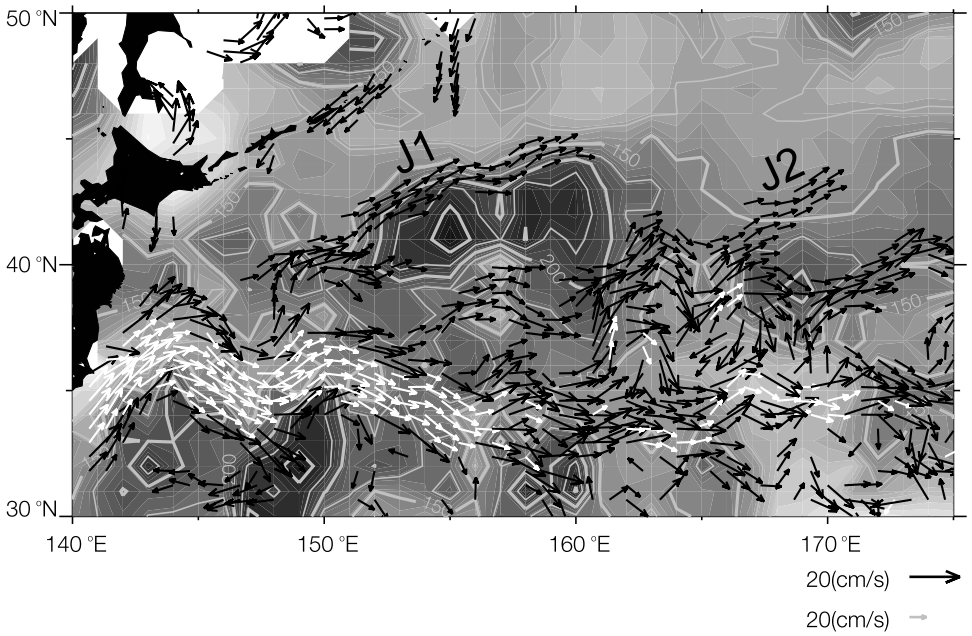

Figure 16. The distribution of late winter (Feb–Mar) mixed layer depth obtained from *Suga et al.* [2004], on which the mean surface currents (>7 cm/s) are superimposed. The location of J1 and J2 is indicated.

over and along the south side of J1. J2, in contrast, weakened after 1999 and mainly changed with an opposite phase to J1, at least in the analyzed period.

[36] Warm tongues and warm streamers, which spread northward from the crests of the KE's meander, are sometimes called the secondary Kuroshio Front [*Kawai*, 1972] and are regarded not only as the main source of warm water transported into MWR but also as a possible mechanism in accelerating the northward migration of pelagic fish in early summer [e.g., *Kawai and Saitoh*, 1986; *Sugimoto and Tameishi*, 1992]. The behavior of these phenomena has been investigated as a series of events or short-term phenomena [*Kawai and Saitoh*, 1986; *Sainz-Trapaga and Sugimoto*, 1998]. The results in this study hypothesize that these short-term secondary Kuroshio Front phenomena, being linked with the KE's variability, systematically connect to J1, which has quasi-stationary and persistent characteristics. In addition, as shown before, since J1 roughly parallels with SAF, the warm tongues driven by J1 play important roles in supplying surface warm water into the subarctic region and, in addition, they might be direct routes for the northward migration of pelagic fishes toward the feeding ground in the subarctic region. The detailed variations, including a mechanism linking them, should be studied in the future by adding numerical simulations.

[37] In order to discuss the vertical structure related to the jets, the hydrographic mean fields were constructed for spatial structure to be held as finely as possible. The flow field relative to 1500 dbar showed the robust structures of J1 and J2 as well as KE, which supports the idea that the warm tongues were driven by the quasi-stationary geostrophic jets. The intermediate flow patterns involved the detour route around the tongue-like protrusion of warm and saline water, connecting between J1 and J2. These jets roughly corresponded to SAF and the front of the Kuroshio mixing ratio (the 30% contours), implying that they probably form a type of boundary between the subtropical and subarctic gyres in the northwestern North Pacific.

[38] It should be noted that the inside of the anticyclonic detour route around the tongue-like intrusion corresponds to the region with the local maximum of late winter mixed water depth (MLD). Figure 16 shows the mixed layer depth map in February [*Suga et al.*, 2004], on which the mean surface currents (>7 cm/s) are superimposed. The winter MLD deeper than 200 m is located south of J1. J1 is roughly consistent with the sharp MLD fronts. This feature can be seen as analogy with the local MLD maximums in the recirculation gyre south of KE (140–150°E, 30–34°N). The maximum of thickness of density range 26.6–27.0 σ_θ has also been reported to appear south of J1 (around 42°N) [*Iwao et al.*, 2003], which is inferred from the density section along 155°E (Figure 15a). In fact, potential vorticity minimum on the 26.6–26.7 σ_θ surfaces is distributed in the same region (not shown). The depth at 26.6–26.7 σ_θ layers in these regions is about 200–250 m (Figure 15a), which is roughly the same depth as the late winter mixed layer. It is thus hypothesized that J1 might play a significant role, through the supply of saline water, in forming low potential vorticity water and a deep mixed layer. Although a detailed discussion is beyond the scope of this study, this is a phenomenon that suggests the possibility for the jets in this study to contribute to water mass formation.

[39] **Acknowledgments.** The authors thank the editor and the two anonymous reviewers for constructive comments and English editing, which were helpful in improving our paper. The authors also thank members of Center for Atmospheric and Oceanic Studies and Physical Oceanography Group at Tohoku University for helpful discussions. This study is supported by Special Coordination Fund for Promoting Science and Technology "New Generation SST" of Ministry of Education, Culture, Sports, Science and Technology (MEXT), Japan, and the Category 7 of MEXT RR2002 "Project for Sustainable Coexistence of Human, Nature

and the EarthRR2002 Symbiosis Project of MEXT, Japan". The altimeter products were produced by Segment Sol multimissions d'ALTimétrie, d'Orbitographie et de localisation précise/Data Unification and Altimeter Combination System (SSALTO/DUACS) as part of the Environment and Climate European Union (EU) ENhanced ocean data Assimilation and Climate prediction (ENACT) project (EVK2-CT2001-00117) and distributed by Archiving, Validation and Interpretation of Satellites Oceanographic data (AVISO), with support from Centre National d'Etudes Spatiales (CNES).

References

Argo Science Team (2001), Argo: The global array of profiling floats, in *Observing the Oceans in the 21st Century*, edited by C. J. Koblinsky and N. R. Smith, pp. 248–258, GODAE Proj. Off., Bur. of Meteorol., Melbourne.

Armstrong, E. M., and J. Vazquez-Cuervo (2001), A new global satellite-based sea surface temperature climatology, *Geophys. Res. Lett.*, *28*, 4199–4202.

Ducet, N., P. Y. Le Traon, and G. Reverdin (2000), Global high resolution mapping of ocean circulation from TOPEX/Poseidon and ERS-1 and -2, *J. Geophys. Res.*, *105*, 19,477–19,498.

Favorite, F., A. J. Dodimead, and K. Nasu (1976), Oceanography of the Subarctic Pacific region, 1960–71, *Bull. Int. North Pac. Comm.*, *33*, 1–187.

Guan, L., and H. Kawamura (2004), Merging satellite infrared and microwave SSTs: Methodology and evaluation of the new SST, *J. Oceanogr.*, *60*, 905–912.

Hurlburt, H. E., and E. J. Metzger (1998), Bifurcation of the Kuroshio Extension at the Shatsky Rise, *J. Geophys. Res.*, *103*, 7549–7566.

Hurlburt, H. E., A. J. Wallcraft, W. J. Schmitz Jr., P. J. Hogan, and E. J. Metzger (1996), Dynamics of the Kuroshio/Oyashio current system using eddy-resolving models of the North Pacific Ocean, *J. Geophys. Res.*, *101*, 941–976.

Isoguchi, O., and H. Kawamura (2003), Eddies advected by time-dependent Sverdrup circulation in the western boundary of the subarctic North Pacific, *Geophys. Res. Lett.*, *30*(15), 1794, doi:10.1029/2003GL017652.

Isoguchi, O., H. Kawamura, and T. Kono (1997), A study on wind-driven circulation in the subarctic North Pacific using TOPEX/POSEIDON altimeter data, *J. Geophys. Res.*, *102*, 12,457–12,468.

Iwao, T., M. Endoh, N. Shikama, and T. Nakano (2003), Intermediate circulation in the northwestern North Pacific derived from subsurface floats, *J. Oceanogr.*, *59*, 893–904.

Japan Meteorological Agency (2001), *Subarctic Gyre Experiment* [CD-ROM], Tokyo.

Johnson, G. C., and M. J. McPhaden (1999), Interior pycnocline flow from the subtropical to the equatorial Pacific Ocean, *J. Phys. Oceanogr.*, *29*, 3073–3089.

Kawai, H. (1972), Hydrography of the Kuroshio Extension, in *Kuroshio: Its Physical Aspects*, edited by H. Stommel and K. Yoshida, pp. 235–352, Univ. of Tokyo Press, Tokyo.

Kawai, H., and S. Saitoh (1986), Secondary fronts, warm tongues and warm streamers of the Kuroshio Extension system, *Deep Sea Res.*, *33*, 1487–1507.

Kawai, Y., H. Kawamura, S. Takahashi, K. Hosoda, H. Murakami, M. Kachi, and L. Guan (2006), Satellite-based high-resolution global optimum interpolation sea surface temperature data, *J. Geophys. Res.*, *111*, C06016, doi:10.1029/2005JC003313.

Kawamura, H., K. Mizuno, and Y. Toba (1986), Formation process of a warm-core ring in the Kuroshio-Oyashio frontal zone - December 1981–October 1982, *Deep Sea Res.*, *33*, 1617–1640.

Kono, T. (1997), Modification of the Oyashio water in the Hokkaido and Tohoku areas, *Deep Sea Res.*, *44*, 669–688.

Kuragano, T., and A. Shibata (1997), Sea surface dynamic height of the Pacific Ocean derived from TOPEX/POSEIDON altimeter data: Calculation method and accuracy, *J. Oceanogr.*, *53*, 585–599.

Levine, E. R., and W. B. White (1983), Bathymetric influences upon the character of North Pacific fronts, 1976–1980, *J. Geophys. Res.*, *88*, 9617–9625.

Levitus, S., and T. P. Boyer (1994), *World Ocean Atlas 1994,* vol. 4, *Temperature*, *NOAA Atlas NESDIS 4*, 117 pp., Natl. Oceanic and Atmos. Admin., Silver Spring, Md.

Levitus, S., R. Burgett, and T. P. Boyer (1994), *World Ocean Atlas 1994,* vol. 3, *Salinity*, *NOAA Atlas NESDIS 3*, 99 pp., Natl. Oceanic and Atmos. Admin., Silver Spring, Md.

Macdonald, A. M., T. Suga, and R. G. Curry (2001), An isopycnally averaged North Pacific climatology, *J. Atmos. Oceanic Technol.*, *18*, 394–420.

Mizuno, K., and W. B. White (1983), Annual and interannual variability in the Kuroshio Current System, *J. Phys. Oceanogr.*, *13*, 1847–1867.

Montgomery, R. B. (1937), A suggested method for representing gradient flow in isentropic surfaces, *Bull. Am. Meteorol. Soc.*, *18*, 210–212.

Niiler, P. P., N. A. Maximenko, G. G. Panteleev, T. Yamagata, and D. B. Olson (2003), Near-surface dynamical structure of the Kuroshio Extension, *J. Geophys. Res.*, *108*(C6), 3193, doi:10.1029/2002JC001461.

NODC (1994), World Ocean Atlas 1994 CD-ROM data set documentation, *Informal Rep. 13*, 30 pp., Natl. Oceanogr. Data Cent.

Qu, T., H. Mitsudera, and B. Qiu (2001), A climatological view of the Kuroshio/Oyashio system east of Japan, *J. Phys. Oceanogr.*, *31*, 2575–2589.

Sainz-Trapaga, S., and T. Sugimoto (1998), Spreading of warm water from the Kuroshio Extension into the Perturbed Area, *J. Oceanogr.*, *54*, 257–271.

Sainz-Trapaga, S. M., G. J. Goni, and T. Sugimoto (2001), Identification of the Kuroshio Extension, its bifurcation and northern branch from altimetry and hydrographic data during October 1992–August 1999: Spatial and temporal variability, *Geophys. Res. Lett.*, *28*, 1759–1762.

Stammer, D. (1997), Steric and wind-induced changes in TOPEX/POSEIDON large-scale sea surface topography observations, *J. Geophys. Res.*, *102*, 20,987–21,009.

Suga, T., K. Motoki, Y. Aoki, and A. M. Macdonald (2004), The North Pacific climatology of winter mixed layer and mode waters, *J. Phys. Oceanogr.*, *34*, 3–22.

Sugimoto, T., and H. Tameishi (1992), Warm-core rings, streamers and their role on the fishing ground formation around Japan, *Deep Sea Res.*, *39*, suppl., S183–S201.

Talley, L. (1993), Distribution and formation of North Pacific Intermediate Water, *J. Phys. Oceanogr.*, *23*, 517–537.

Uehara, K., H. Miyake, and M. Okazaki (1997), Characteristics of the flows in the Oyashio area off Cape Erimo, Hokkaido, Japan, *J. Oceanogr.*, *53*, 93–103.

Yasuda, I. (2003), Hydrographic structure and variability in the Kuroshio-Oyashio transition area, *J. Oceanogr.*, *59*, 389–402.

Yasuda, I., K. Okuda, and M. Hirai (1992), Evolution of a Kuroshio warm-core ring-variability of the hydrographic structure, *Deep Sea Res.*, *39*, S131–S161, suppl.

Yuan, X., and L. D. Talley (1996), The subarctic frontal zone in the North Pacific: Characteristics of frontal structure from climatological data and synoptic surveys, *J. Geophys. Res.*, *101*, 16,491–16,508.

Zhang, R. C., and K. Hanawa (1993), Features of the water-mass front in the northwestern North Pacific, *J. Geophys. Res.*, *98*, 967–975.

O. Isoguchi and H. Kawamura, Center for Atmospheric and Oceanic Studies, Graduate School of Science, Tohoku University, Aoba, Sendai, Miyagi 980-8578, Japan. (isoguchi.osamu@jaxa.jp)

E. Oka, Ocean Research Institute, University of Tokyo, 1-15-1 Minamidai, Nakano, Tokyo 164-8639, Japan.